Experimental and numerical investigation of micro-fluid channel designed by topology optimization

Hao LI, Sheng PAN, Xiaohong DING*, Dalei JING, Min Xiong

School of Mechanical Engineering, University of Shanghai for Science and Technology, Shanghai, 200093, China

ABSTRACT

In order to study the relationship between the flow and thermal performances and the layout of cooling channels designed by topology optimization from the engineering point of view, two types of channel layouts with different channel volume fractions are studied. The first is to achieve the minimization of power dissipation under the flow rate quality constraints, and the second is to achieve the maximization of heat exchange under the constant input power constraint. Then the optimized heat sinks together with the conventional S-shaped channel heat sinks are manufactured and their flow and thermal performances are investigated both numerically and experimentally. The results reveal that the optimized channel design can enhance the flow and thermal performances of the heat sinks. The power dissipation minimization design provides the best temperature uniformity, while the heat exchange maximization design keeps the peak temperature to a minimum. Additionally, the coefficient of performance of the heat exchange maximization design is the highest among three types of layouts, which means it can remove more heat energy at the same pumping power.
Key words: Topology optimization, Power dissipation minimization, Heat exchange maximization, Liquid cooled heat sink.

1. INTRODUCTION

As a key component of MEMS, microprocessor with high computing performances is facing with severe thermal challenge due to the increasing power density, miniaturization as well as higher operating temperature requirements, and thermal management in corresponding fields has become one of the crucial issues [1]. Recently, the commonly used thermal control techniques include phase-change cooling [2-5] and liquid-cooled heat sink [6-8], etc. Though phase-change cooling utilizes the enthalpy of vaporization, phase-change cooling mechanisms are basically constraint by the critical heat flux [9]. Micro channel heat sink integrated single-phase liquid cooling shows great potential regarding to the excellent heat dissipation capacity and low cost [10]. However, the conventional micro cooling channel layout like parallel or serpentine (S-shaped) pattern has several significant drawbacks such as higher hydraulic resistance and higher temperature gradient, which means higher pumping power is required to remove high heat flux. In order to overcome these disadvantages of the conventional heat sink, the channel layout should be optimally designed to achieve better flow and thermal performances.

To design optimal channel layout with desirable flow and thermal performances, a flexible design method termed topology optimization can be used to develop the cooling channel layout. Topology optimization method was first introduced by Bendsøe and Kikuchi [11] in 1988 for mechanical element design. In 2003, Borrval and Petersson [12] extended this method from structural design to the fluid flow optimization. Since their pioneering work, this method was quickly extended to the steady-state Navier –Stokes flow problems by Olesen et al.

[13], in which the nonlinear topology optimization was implemented with a high-level programming language based on the commercial software package Femlab. Liu et al. [14] analyzed the problem of the fluid topology optimization with flow rate equality constraints. The equality boundaries on the specified boundaries were implemented using the lumped Lagrange multiplier method. Several other studies also reported the successful implementation of topology optimization in different flow states: Darcy-Stokes flows [15], unsteady Navier-Stokes flows [16], and non-Newtonian flows [17]. Additionally, topology optimization is also feasible for the optimization of heat conduction problem, also known by bi-material volume-to-point problems. For a volume of lower conductivity material that is continuously generating heat, topology optimization can arrange the optimal layout of higher conductivity material to remove maximum amount of heat being generated [18, 19]. Finally, for the coupled thermal-fluid problem, there were several attempts of applying topology optimization to the liquid-cooled heat sink design. Koga et al. [20] presented a complete cycle development of a liquid-cooled heat sink designed by topology optimization for best hydraulic-thermo performances, including minimization of power dissipation in fluid flow and maximization of heat dissipation effect. Matsumori [21] conducted the density-based topology optimization under both temperature dependent and temperature independent heat conditions, in which they proposed a way to control the input power by introducing an extra integral equation. Several other topology optimization methods such as level set boundary expressions [22] and Lattice Boltzmann method [23] were also proved to design liquid-cooled heat sink channel layout.

As mentioned above, the design problem of channel layout for heat sinks has attracted a lot of interest of researchers, but there is few study to concern the relationship between the flow and thermal performances, such as the temperature uniformity, maximum heat exchange efficiency, etc., and the layout of channels from the engineering point of view. This paper numerically and experimentally studies this problem. The optimized channel layouts designed by density-based topology optimization method consist two types: (1) a fluid field with optimal uniformity by minimizing power dissipation under flow rate equality constraints; (2) the optimal cooling efficiency with minimum pumping power by maximizing heat exchange through the fluid-solid boundaries. A serpentine-shaped (S-shaped) cooling channel layout is employed as a competitive design case. The experimental investigation is carried out to verify the simulation results of the flow and thermal parameters together with the temperature distribution of the heat sinks. Hence, the flow and thermal performances including the peak temperature and maximum temperature difference and the cooling efficiency of the heat sinks are respectively analyzed.

2. TOPOLOGY OPTIMIZATION DESIGN OF HEAT SINKS

2.1 Fluid topology optimization problem se tting

The design domain is modeled with an i dealized porous media, a body force term F relative to the inverse permeability α with th e function $F = -\alpha\mathbf{u}$ is introduced to the mo mentum equation, where $\mathbf{u}$ is the velocity ve ctor. During the finite element discretization, each element is assigned a local design varia ble γ. The design variable γ continuously var ies from zero to one. For the element where γ=0, $\alpha\to\infty$, $F\to\infty$, stands for the solid dom ain while the blue subdomain where γ=1, α $\to$0, $F\to$0, stands for the fluid domain.

2.2 Governing equations

2.2.1 Flow field

Continuity equation:

$$\nabla^* \cdot \mathbf{u}^* = 0, \tag{1}$$

N-S equation:

$$\left(\mathbf{u}^* \cdot \nabla^*\right)\mathbf{u}^* = \nabla^*\left[-p^*\mathbf{I} + \frac{1}{\mathrm{Re}}\left(\nabla^*\mathbf{u}^* + \left(\nabla^*\mathbf{u}^*\right)^T\right)\right] + F^*, \tag{2}$$

where $\mathbf{u}^*$ and p^* is the dimensionless velocity and pressure, Re is the Reynolds number, F^* is a dimensionless body force term, which represents the friction force due to the porous medium in the fluid flow. Based on the Darcy law, the friction force is proportional to the velocity $\mathbf{u}$, therefore can be formulated as:

$$F^* = -\alpha^* \mathbf{u}^*, \tag{3}$$

where α^* is the dimensionless inverse permeability of a porous medium[12]. $\alpha^*(x)$ is interpreted as a continuous mapping determined by the design variable γ using a interpolation function as follows:

$$\alpha^*(x) = \alpha^*_{\max} \frac{q(1-\gamma)}{q+\gamma}, \tag{4}$$

where q is the penalty factor used for tuning the function shape of $\alpha^*(x)$.

2.2.2 Conjugate heat transfer

Energy equation:

$$\begin{aligned} \mathrm{Re}\,\mathrm{Pr}\left(\mathbf{u}^* \cdot \nabla^*\right) T^* &= \nabla^{*2} T^*, && \text{(in fluid domains)} \\ 0 &= \nabla^{*2} T^* + Q^*, && \text{(in solid domains)} \end{aligned} \tag{5}$$

Where Pr is the Prandtl number, T^* is the dimensionless temperature, Q^* is the dimensionless heat generation which is dependent on the local temperature, as defined in the form of Newton's law of cooling which states the rate of heat loss of a body is directly proportional to the difference in the temperatures between the body and its surroundings [21]:

$$Q^* = h^*\left(1 - T^*\right), \tag{6}$$

where h^* is the dimensionless coefficient that controls the heat generation according to:

$$h^* = \frac{hL^2}{k_f}, \tag{7}$$

where h is the heat generation coefficient which is the proportionality constant between the heat flux and the thermodynamics driving force for the flow of heat.

In this study, the penalty factor q and $\alpha_{max}{}^*(x)$, which are used to control the interpolation of γ, are set to 10^{-2} and10^4, respectively. The Prandtl number Pr is set to 6.78 assuming the coolant fluid is water at 20°C under standard atmosphere pressure neglecting temperature variation. The dimensionless heat generation coefficient h^* and Reynolds number Re is set to 10 and 50, respectively.

2.3 Minimization of power dissipation

2.3.1 Flow field

First, the flow distribution problem is studied to generate a flow field as well as a temperature field with an optimal uniformity. In this example, the channel layout with flow rate constraints on the specified boundaries is optimized based on the power dissipation minimization problem. The design model is depicted in **Fig. 1** where the design domain is shown as blue subdomain, and the specified boundaries with the flow rate equality constraints are represented by a set of white bars. The branch channels are bifurcated in such a way that the ratio of the flow rates $FR_i \in [0,1]$ at boundary Γ_i in the same cross section have to be equal. Thus, the flow rate constraints are specified at the boundaries Γ_i (i=1, 2,…, 16) as FR_1= FR_{16}=1/2, FR_2= FR_{14} =1/3, FR_3= FR_{15}=1/6, FR_4= FR_5= FR_{12}= FR_{13} =1/4, FR_6= FR_7= FR_9= FR_{10}=1/5, FR_8= FR_{11} =1/10, respectively. The upper bound for the constraint of the volume fraction $V_f \in [0,1]$ is chose to V_f =0.4 and V_f =0.6, separately.

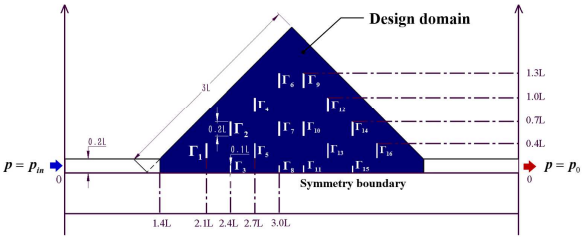

Fig. 1. Design model in the power dissipation minimization problem.

2.3.2 Optimization mathematical model

In this note, power dissipation proposed by Borrvall and Petersson [12] is used as the objective function. Following the research by Liu et al. [14], the specified boundaries are subjected to the flow rate equality constraints. An integral equation with respect to the inlet pressure p^*_{in} is introduced to keep the constant input power [21]. The optimization mathematic model is formulated as follows:

$$\begin{aligned} \underset{\gamma \in [0,1]}{\text{minimize}} \quad & \Phi = \int_\Omega \left[\nabla^* \mathbf{u}^* \cdot \left(\nabla^* \mathbf{u}^* + \nabla^* \mathbf{u}^{*T} \right) + \alpha^* \mathbf{u}^* \cdot \mathbf{u}^* \right] d\Omega, \\ s.t. \quad & \int_\Omega \gamma \, d\Omega \le V_f \cdot Vol_\Omega, \\ & \int_{\Gamma_i} \mathbf{u}^* \cdot \mathbf{n} \, d\Gamma_i = FR_i \cdot \dot{V}_{in}, \ \text{i=1,...,n}, \\ & \int_{\Gamma_{in}} p^*_{in} \, u^* \, d\Gamma = 1, \end{aligned} \tag{8}$$

where Ω is the design domain, Vol_Ω is the volume of the whole design domain, Φ is the optimization

objective. $\dot{V}_{in}$ denotes to the flow rate at the inlet boundary Γ_{in}, and **n** is the outward normal vector of the boundary.

The velocity and pressure field in the objective function is solved through the fluidic analysis defined by Eqs. (1) and (5).

The forward problems and the optimization processes are implemented using a finite element software COMSOL Multiphysics [24]. A gradient-based optimization method sequential quadratic optimization (SNOPT) is employed to solve the optimization problem, which is built in the software package. The optimization iterations stopped when the criteria of $|\Phi_{k+1}-\Phi_k|<1\times10^{-6}$ is satisfied.

2.3.3 Optimal Channel layout

The optimization converged after 37 steps. The dimensions of the conceptual design for V_f =0.4 and V_f =0.6 are presented in **Fig. 2**. It can be observed that the channel layouts have a net-shaped appearance, and the channel layout for V_f=0.6 has smaller islands and wider flow channels than those for the case of V_f=0.4.

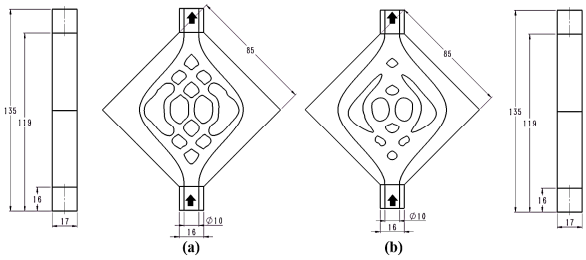

Fig. 2. Dimensions of the heat sinks with the power dissipation minimization channel design (a) V_f =0.4 and (b) V_f =0.6.

2.4 Maximization of heat exchange

2.4.1 Optimization problem setting

Next, the channel layout is optimized based on the heat exchange maximization problem. The design model is illustrated in **Fig. 3**, in which case the conjugate heat transfer is considered. The initial value of the design variable γ is set to 1, namely the design domain is initialized as fluid. The total number of triangular elements reaches 9326. The upper bound for the constraint of the volume fraction of γ is chose to V_f =0.4 and V_f =0.6, separately. The inlet temperature T_{in} is set to 0 K.

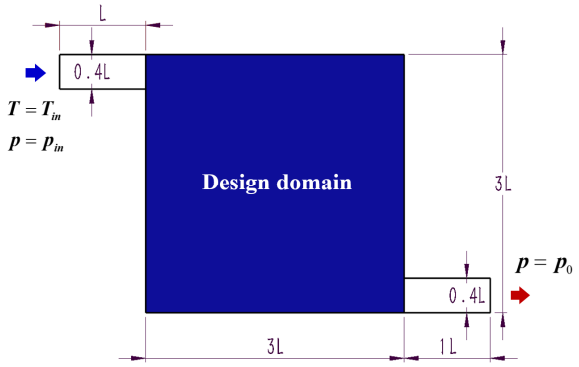

Fig. 3. Design model in the heat exchange ma ximization problem.

2.4.2 Optimization mathematical model

Basically, the heat energy is generated from the heat source, then transferred through solid-fluid boundaries, and the heat energy can be removed by the fluid flowing through the channel so that the thermal balance can be achieved. Therefore, the objective function is given by [21] which represents the total amount of the heat exchange through the fluid-solid boundaries. The optimization is subjected to the volume constraint and the constant input power defined as follows:

$$\begin{aligned} &\underset{\gamma\in[0,1]}{\text{maximize}} \quad \Phi=\int_\Omega(1-\gamma)h^*(1-T^*)\,d\Omega, \\ &s.t. \qquad \int_\Omega\gamma\,d\Omega\le V_f\cdot Vol_\Omega, \\ &\qquad\quad \int_{\Gamma_{\text{in}}}p_{in}^*\,u^*\,d\Gamma=1. \end{aligned} \tag{9}$$

The temperature field in the objective functi on is solved through the coupled thermal-flui d analysis defined by Eqs. (1), (2) and (5).

2.4.3 Optimization channel layout

The optimization converged after 188 steps. It can be observed that the optimized fluid channels for the case of V_f=0.6, as shown in **Fig. 4**(b), become narrower and more bifurcated in comparison to those for the case of V_f =0.4, as shown in **Fig. 4**(a).

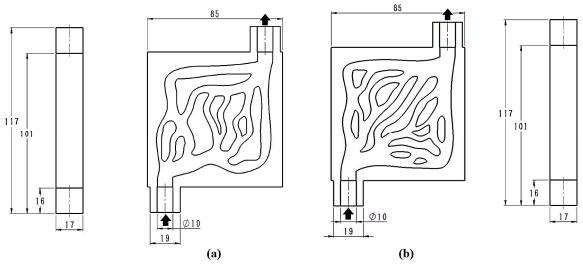

Fig. 4. Dimensions of the heat sinks with the heat exchange maximization channel design (a) V_f =0.4 and (b) V_f =0.6.

2.5 Competitive design case of heat sinks with S-shaped cooling channels

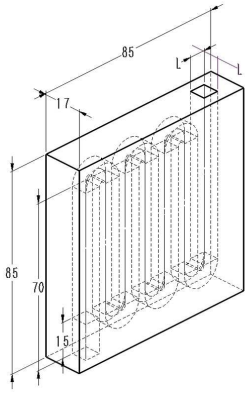

Fig. 5. Dimensions of the heat sink with S-shaped cooling channel design.

Next, a competitive design case with conventional channel layout is introduced to compare the flow and thermal performances with the heat sinks designed by topology optimization. In order to uncover the effects of volume fraction, V_f is also set to 0.4 and 0.6, separately. The different volume fractions are obtained by varying the cross section area of the channels while the number and the length of the channels are fixed. The length L is set to L=7.0 mm and L=7.5 mm for the case of V_f=0.4 and V_f=0.6, respectively. Details about the dimensions are shown in **Fig. 5**.

3. NUMERICAL AND EXPERIMENTAL VERIFICATION

3.1 Manufacture of heat sinks

To experimentally investigate the flow and thermal performances of the heat sinks with different channel layouts: the S-shaped design, the power dissipation minimization design, and the heat exchange maximization design, the heat sinks are manufactured as shown in **Fig. 6**. During the experiments, the Aluminum heat sink is placed on the heating unit, and thermal insulation aerogel is wrapped around the plate. Furthermore, the top surface of the Aluminum heat sink is coated with thermal silicone grease so that misreading from the infrared camera caused by the reflective effect of Aluminum surface can be eliminated.

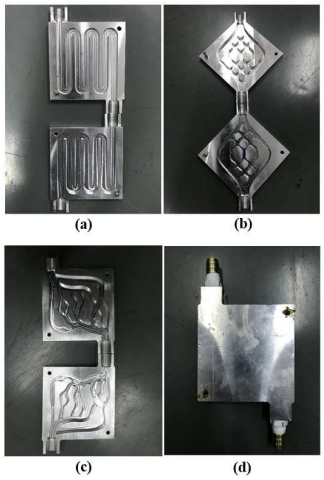

Fig. 6. The open form of the heat sinks with (a) the S-shaped design, (b) the power dissipat ion minimization design, and (c) the heat exch ange maximization design. (d) The closed for m of the heat sink.

3.2 Experimental setup

Next, the experimental system is built, as shown in **Fig. 7**. The system comprises of three major parts: coolant circulation unit, testing unit and heating unit. Coolant circulation is achieved by driving de-ionized water using an industrial chiller. A ball valve and a needle valve are used to regulate the flow rate coarsely or finely, and the peak output volumetric flow rate of the coolant can be up to 16 L/min. For the testing unit, a volumetric flowmeter is embedded in the coolant line to measure the flow rate of the coolant. A differential pressure sensor is connected with the heat sink in parallel to measure the pressure drop between the inlet and outlet ports of the heat sink.

PT100 temperature sensors are inserted into the inlet and outlet channels to measure the inlet and outlet temperature. The temperature distribution over the certain surface of the heat sink is observed by an Infrared Camera. The heating unit consisting of the red copper plate embedded stainless heating bars is used to apply constant heat flux on the surface of the heat sink, and the schematic of the heating unit is shown in **Fig. 7**(b). A voltage regulator is used to adjust the heating power and the resulting heat flux.

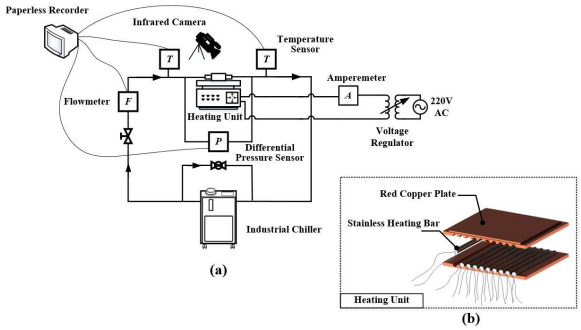

Fig. 7. The schematic of (a) the experimental system, and (b) heating unit.

3.3 Simulation modeling and experimental verification

To compare the numerical and experimental results, the simulation analysis is set to be exactly the same as the experimental setup. The coolant is de-ionized water while the materials of the each heat sink is Aluminum 6061. The boundary conditions of the simulation are also the same as the experimental setup and as follows: (1) Inlet and outlet: a constant pressure difference Δp between the inlet and outlet of the heat sink is applied over the heat sink, and the inlet temperature of the coolant is 20°C. (2) Interface: the solid-liquid interface satisfies no-slip velocity boundary condition, temperature continuity and relates to the temperature gradients. (3) Wall: a constant heat flux q'' is applied at the bottom wall of the heat sink and all other walls are adiabatic.

The simulation results are validated by comparing with the experimental data. Both the experimental and numerical results regarding the effects of pressure drop on the peak temperature and the flow rate of three heat sinks with different types of channel layouts are given in **Fig. 8**, which shows that the numerical results is in well agreement with the experimental results. The maximum relative errors of the peak temperature and the flow rate are less than 3.35% and 6.63%, respectively. Thus, it can be concluded that both the experimental and numerical results are correct.

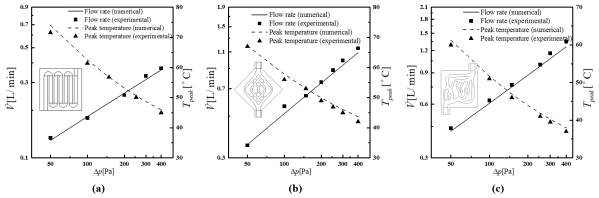

Fig. 8. Numerical and Experimental results of the variations in the peak temperature and flo w rate relative to the pressure drop for (a) the S-shaped design, (b) the power dissipation mi nimization design, and (c) the heat exchange maximization design, with the channel volume fraction of V_f=0.4, under the heat flux of q'' =50 kW/m^2.

3.4 Results and discussion

3.4.1 Thermal performances

Thermal parameters including the temperature distribution, the peak temperature and the temperature uniformity are studied to analyze the thermal performances of heat sinks with three types of channel design exposing to a constant heat flux. Note that the temperature uniformity is evaluated by the maximum temperature difference ΔT_{max} observed on heat sink surface [25, 26].

Fig. 9 presents the temperature distributio ns for the three competing designs with differ ent channel volume fractions given by the nu merical and experimental studies. The tempera ture distributions in **Fig. 9** show the agreemen t between the numerical and experimental resu lts. In addition, as for each type of channel de sign, the temperature distributions for different volume fractions (V_f=0.4 and V_f=0.6) are simi lar to each other except the absolute value of the temperature due to the similar cooling cha nnel layout. **Fig. 9**(a) shows that the peak tem perature for the S-shaped channel design locat es close to the outlet port. When the pressure drop is Δp=200 Pa, the value of the T_{peak} and

ΔT_{max} decreases 13.0% and 18.8% respectively in the case of V_f=0.6 in comparison to the ca se of V_f=0.4. This is because that the wider c ooling channels for the case of a larger chann el volume fraction has a smaller hydraulic resi stance and leads to a larger flow rate under th e fixed pressure drop , and hence decreases th e thermal resistance and the resulting T_{peak} and ΔT_{max}. **Fig. 9**(b) reveals that the peak temperat ure on the power dissipation minimization des ign are located at the two corners where there is less coolant with a relatively lower speed c ompared with the central area. Similar to the S-shaped channels, the value of the T_{peak} and ΔT_{max} decreases 7.31% and 16.4% in the case of V_f=0.6 in comparison to the case of V_f=0. 4 under the pressure drop of 200 Pa due to th e same mechanisms. Note that the temperature is distributed symmetrically due to the symme try of the cooling channel layout. **Fig. 9**(c) sh ows that the peak temperature on the heat exc hange maximization design occurs at the corn er opposite to the outlet port. However, the va lue of the T_{peak} and ΔT_{max} increases 1.37% and 5.63% in the case of V_f=0.6 in comparison to the case of V_f=0.4. The reason for this increa se is due to the narrower and denser cooling channels obtained by optimization process.

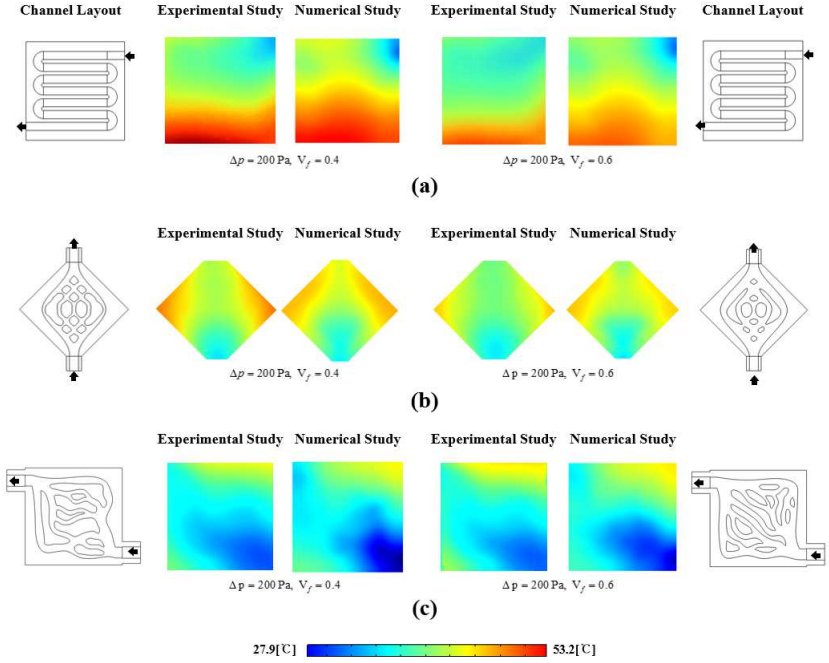

Fig. 9. Temperature distributions of (a) the S-shaped channels design, (b) the power dissipation minimization design, and (c) the heat exchange maximization design for experimental and numeri cal studies with the heat flux of q''=50 kW/m^2.

4. CONCLUSIONS

In this paper, the design problem of channel layout embedded in the heat sinks is studied numerically and experimentally. The relationship between the flow and thermal performances, including the temperature uniformity and maximum heat exchange efficiency, and the cooling channel layouts designed by topology optimization is discussed from the engineering point of view. First, two types of optimized channel layouts are generated by density-based topology optimization: (1) a fluid field with optimal uniformity by minimizing power dissipation under flow rate equality constraints; (2) the optimal cooling efficiency with minimum pumping power by maximizing heat exchange through the fluid-solid boundaries. For each type of cooling channel, two different volume fractions of the cooling channel are considered. Next, the experimental investigation is conducted to verify the numerical results of the flow and thermal parameters together with the temperature distribution of the heat sinks. Finally, the flow and thermal performances including the peak temperature, maximum temperature difference, and the cooling efficiency of the heat sinks are

analyzed. The results can be concluded as follows: (1) The cooling channel designed with heat exchange maximization can provide the lowest peak temperature among the three competing designs, which is more significant for small channel volume due to the lowest hydraulic resistance. (2) The cooling channel designed with power dissipation minimization can achieve the lowest temperature difference on the heat sinks, which is more apparent for the large channel volume, because a fluid field with optimal uniformity can be obtained. In conclusion, the heat sink with topology optimized fluid cooling channel is an effective approach to enhance the flow and thermal performances, and can be applied to the thermal management of microprocessors to achieve an optimal performances.

REFERENCES

1. A. Bartolini, M. Cacciari, M. Tilli, L. Benini, Thermal and Energy Management of High-Performance Multicores: Distributed and Self-Calibrating Model-Predictive Controller. IEEE Trans. Parallel Distrib. 24 (2013) 183.
2. C. Woodcock, X. Yu, J. Plawsky, Y. Peles, Piranha Pin Fin (PPF) — Advanced flow boiling microstructures with low surface tension dielectric fluids. Int. J. Heat Mass Transfer 90 (2015) 591-604.
3. G. Nagayama, S. Gyotoku, T. Tsuruta, Thermal performance of flat micro heat pipe with converging microchannels. Int. J. Heat Mass Transfer 122 (2018) 375-382.
4. B. Kelly, Y. Hayashi, Y.J. Kim, Novel radial pulsating heat-pipe for high heat-flux thermal spreading. Int. J. Heat Mass Transfer 121 (2018) 97-106.
5. M. Najim, M.B. Feddaoui, A. Nait Alla, A. Charef, A.E. Kabeel, New cooling approach using successive evaporation and condensation of a liquid film inside a vertical mini-channel. Int. J. Heat Mass Transfer 122 (2018) 895-912.
6. W. Escher, B. Michel, D. Poulikakos, Efficiency of optimized bifurcating tree-like and parallel microchannel networks in the cooling of electronics. Int. J. Heat Mass Transfer 52 (5) (2009) 1421-1430.
7. X. Luo, Z. Mao, Thermal modeling and design for microchannel cold plate with high temperature uniformity subjected to multiple heat sources. Int. Commun. Heat Mass Transf. 39 (39) (2012) 781–785.
8. A. Sakanova, C.C. Keian, J. Zhao, Performance improvements of microchannel heat sink using wavy channel and nanofluids. Int. J. Heat Mass Transfer 89 (2015) 59-74.
9. A. Jaikumar, S.G. Kandlikar, Pool boiling enhancement through bubble induced convective liquid flow in feeder microchannels. Appl. Phys. Lett. 108 (4) (2016) 241603.
10. Z. Lu, T.R. Salamon, S. Narayanan, K.R. Bagnall, D.F. Hanks, D.S. Antao, B. Barabadi, J. Sircar, M.E. Simon, E.N. Wang, Design and Modeling of Membrane-Based Evaporative Cooling Devices for Thermal Management of High Heat Fluxes. IEEE Trans. Compon. Packag. Technol., 6 (7) (2016) 1056-1065.
11. M.P. Bendsøe, N. Kikuchi, Generating optimal topologies in structural design using a homogenization method. Comput. Methods Appl. Mech. 71 (2) (1988) 197-224.
12. T. Borrvall, J. Petersson, Topology optimization of fluids in Stokes flow. Int. J. Numer. Methods Fluids 41 (1) (2003) 77-107.
13. L.H. Olesen, F. Okkels, H. Bruus, A high-level programming-language implementation of topology optimization applied to steady-state Navier–Stokes flow. Internat. J. Numer. Methods Engrg. 65 (7) (2006) 975-1001.
14. Z. Liu, Q. Gao, P. Zhang, M. Xuan, Y. Wu, Topology optimization of fluid channels with flow rate equality constraints. Struct Multidisc Optim. 44 (1) (2011) 31-37.
15. J.K. Guest, J.H. Prévost, Topology optimization of creeping fluid flows using a Darcy–Stokes finite element. Int. J. Numer Methods Eng. 66 (3) (2006) 461-484.
16. Y. Deng, Z. Liu, P. Zhang, Y. Liu, Y. Wu, Topology optimization of unsteady incompressible Navier-Stokes flows. J.Comput.Phys. 230 (17) (2011) 6688-6708.
17. Pingen, Georg, Maute, Kurt, Optimal design for non-Newtonian flows using a topology optimization approach. Comput. Math. Appl. 59 (7) (2010) 2340-2350.
18. S.H. Wei, L.G. Chen, F.R. Sun, "Volume-Point" heat conduction constructal optimization with entransy dissipation minimization objective based on rectangular element. Sci. China, Ser. E 51 (8) (2008) 1283-1295.
19. S. Wei, L. Chen, F. Sun, The area-point constructal optimization for discrete variable cross-section conducting path. Appl. Energy 86 (7–8) (2009) 1111-1118.
20. A.A. Koga, E.C.C. Lopes, H.F.V. Nova, C.R.D. Lima, E.C.N. Silva, Development of heat sink device by using topology optimization. Int. J. Heat Mass Transfer 64 (3) (2013) 759-772.
21. T. Matsumori, T. Kondoh, A. Kawamoto, T. Nomura, Topology optimization for fluid–thermal interaction problems under constant input power. Struct Multidisc Optim. 47 (4) (2013) 571-581.
22. K. Yaji, T. Yamada, S. Kubo, K. Izui, S. Nishiwaki, A topology optimization method for a coupled thermal–fluid problem using level set boundary expressions. Int. J. Heat Mass Transfer 81 (2015) 878-888.
23. K. Yaji, T. Yamada, M. Yoshino, T. Matsumoto, K. Izui, S. Nishiwaki, Topology optimization in thermal-fluid flow using the lattice Boltzmann method. J.Comput.Phys. 307 (2015) 355-377.
24. COMSOL Multiphysics 5.3a, COMSOL Inc., 2017.
25. K.H. Cho, J. Lee, H.S. Ahn, A. Bejan, M.H. Kim, Fluid flow and heat transfer in vascularized cooling plates. Int. J. Heat Mass Transfer 53 (19-20) (2010) 3607-3614.
26. K.H. Cho, W.P. Chang, M.H. Kim, A numerical and experimental study to evaluate performance of vascularized cooling plates. International Journal of Heat & Fluid Flow 32 (6) (2011) 1186-1198.
27. C. Xia, J. Fu, J. Lai, X. Yao, Z. Chen, Conjugate heat transfer in fractal tree-like channels network heat sink for high-speed motorized spindle cooling. Appl. Therm. Eng. 90 (2015) 1032-1042.